Resolving the energy paradox of chaperone/usher-mediated fibre assembly

Anton V. ZAVIALOV*[1], Vladimir M. TISCHENKO†[2], Laura J. FOOKS‡, Bjørn O. BRANDSDAL§[3], Johan ÅQVIST§, Vladimir P. ZAV'YALOV‖, Sheila MacINTYRE‡ and Stefan D. KNIGHT*[1]

*Department of Molecular Biology, Uppsala Biomedical Center, Swedish University of Agricultural Sciences, Box 590, SE-753 24 Uppsala, Sweden, †Institute of Biological Instrumentation, 142292 Pushchino, Russian Federation, ‡Microbiology Division, School of Animal and Microbial Sciences, University of Reading, Reading RG6 6AJ, U.K., §Department of Cell and Molecular Biology, Uppsala Biomedical Center, Uppsala University, Box 596, SE-751 24 Uppsala, Sweden, and ‖Department of Molecular and Microbial Biology, George Mason University Manassas, VA 20110, U.S.A.

Periplasmic chaperone/usher machineries are used for assembly of filamentous adhesion organelles of Gram-negative pathogens in a process that has been suggested to be driven by folding energy. Structures of mutant chaperone–subunit complexes revealed a final folding transition (condensation of the subunit hydrophobic core) on the release of organelle subunit from the chaperone–subunit pre-assembly complex and incorporation into the final fibre structure. However, in view of the large interface between chaperone and subunit in the pre-assembly complex and the reported stability of this complex, it is difficult to understand how final folding could release sufficient energy to drive assembly. In the present paper, we show the X-ray structure for a native chaperone–fibre complex that, together with thermodynamic data, shows that the final folding step is indeed an essential component of the assembly process. We show that completion of the hydrophobic core and incorporation into the fibre results in an exceptionally stable module, whereas the chaperone–subunit pre-assembly complex is greatly destabilized by the high-energy conformation of the bound subunit. This difference in stabilities creates a free energy potential that drives fibre formation.

Key words: assembly, chaperone, chaperone/usher pathway, protein stability, protein folding.

INTRODUCTION

Most Gram-negative pathogens express adhesive surface organelles that allow them to specifically target and bind to host tissues and cause infection. A periplasmic chaperone/usher machinery is used for the controlled assembly of many such organelles [1–4]. The periplasmic chaperones bind nascent organelle subunits as they enter the periplasm via the Sec pathway, and protect them from non-productive aggregation and proteolytic degradation by capping their assembly surfaces. Binary chaperone–subunit pre-assembly complexes are targeted to the outer membrane usher where subunits are released from the chaperone and assembled into linear fibres that are secreted through the usher pore to the cell surface.

Structures of several periplasmic chaperone–subunit complexes are available [5–8]. The subunits have an incomplete immunoglobulin-like fold in a six-stranded β-sandwich. The incomplete fold precludes the formation of a closed hydrophobic core, leaving a surface-exposed hydrophobic 'acceptor' cleft between the two sheets at the edge of the subunit (Figure 1). The chaperone binds by capping this cleft to form a superbarrel with an extensive chaperone–subunit interface and a joint hydrophobic core [8]. In the superbarrel, the chaperone G_1 donor strand occupies the acceptor cleft, with the large hydrophobic residues from the G_1 donor strand inserted between the two sheets of the subunit β-sandwich, preventing them from contacting each other. For this reason, the chaperone-bound conformation is referred to as the 'open' or 'expanded' conformation.

The recently reported structure of a Caf1M–Caf1′–Caf1″ (where Caf1M is the chaperone involved in *Yersinia pestis* capsule assembly, Caf1′ is the chaperone-bound F1 antigen subunit and Caf1″ is the subunit in its final fibre conformation) complex [8] with the minimal *Y. pestis* F1-antigen fibre (Caf1′–Caf1″) bound to Caf1M revealed that fibre subunits are linked together by DSC (donor strand complementation) [5,6] with an N-terminal G_d donor strand segment of one subunit inserted into the hydrophobic cleft of a neighbouring subunit [8] (Figure 1). The resulting linear fibre is composed of globular modules each having an intact Ig topology generated by DSC. The generality of this mode of interaction is supported by the crystal structure of a P pilus subunit, PapE, in complex with a peptide corresponding to the N-terminal region of PapK [7]. The morphology of surface organelles is determined by coiling of the secreted linear Ig-module fibres into structures of different architecture [9].

No energy input from external sources is required to convert periplasmic chaperone–subunit pre-assembly complexes into free chaperone and secreted fibres [10], in spite of a much more extensive interface between chaperone and subunit than between fibre subunits [8]. Some clues as to how the process can be energetically driven have been suggested by structural studies [7,8]. Comparison of Caf1′ with Caf1″ revealed a large conformational difference. In contrast with the large hydrophobic donor residues in the chaperone G_1 donor strand, the much smaller donor residues in the subunit N-terminal G_d donor segment do not intercalate between the two sheets of the subunit β-sandwich, allowing close contact between the two sheets (Figure 1). Therefore the

Abbreviations used: Caf1M, chaperone involved in *Yersinia pestis* capsule assembly; Caf1′ and Caf1″, polypeptide subunit of capsule in chaperone-bound and fibre conformations respectively; Caf1-SC, self-complemented subunit; C_p, partial heat capacity of the protein; DSC, donor strand complementation; GdmCl, guanidinium chloride; ΔG, free energy of unfolding; ΔH^{vH}, van't Hoff enthalpy; IEF, isoelectric focusing; MD, molecular dynamics; R.M.S.D., root mean square deviation; T_0, upper limit value for the melting temperature; T_m, melting temperature; WT, wild-type.

[1] Correspondence may be addressed to either of these authors (email anton.zavialov@molbio.slu.se or stefan.knight@molbio.slu.se).
[2] Present address: Institute of Protein Research, 142292 Pushchino, Russian Federation.
[3] Present address: Norwegian Structural Biology Centre, University of Tromsø, N9037 Tromsø, Norway.

Atomic co-ordinates for the native Caf1M–Caf1′–Caf1″ complex have been deposited in the Protein Data Bank under accession code 1Z9S.

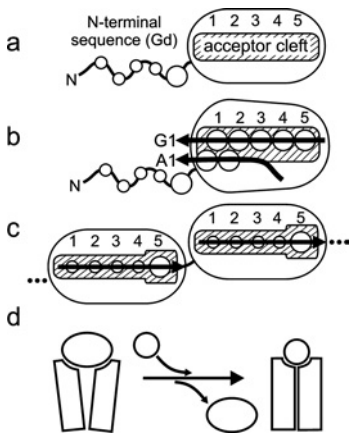

Figure 1 Schematic illustration of DSC

(**a**) Hypothetical free Caf1 subunit. The non-complemented subunit contains a hydrophobic acceptor cleft with five subsites for the insertion of five side chains of a donor strand. The N-terminal donor strand segment of Caf1 is unstructured. (**b**) Complex with Caf1M. Two chaperone strands (A_1 and G_1) interact with edge strands of the subunit to form a superbarrel [8]. Large G_1 and A_1 (partially) donor residues insert into the acceptor cleft between the two sheets of the subunit β-sandwich such that the superbarrel acquires a fused hydrophobic core. (**c**) Fibre. Consecutive subunits form Ig-like fibre modules by insertion of the N-terminal G_d donor strand of one subunit into the hydrophobic acceptor cleft of a neighbouring subunit. (**d**) Donor strand exchange. On release of the subunit from the chaperone and incorporation into the fibre, the two sheets of the subunit β-sandwich move together to form a close packed subunit hydrophobic core. In (**a**), (**b**) and (**c**), side chains participating in DSC are shown as spheres with radii reflecting the size of the donating groups (methyl and larger).

fibre conformation is also referred to as the 'closed' or 'condensed' conformation. The observed difference between open and closed conformations, involving a rearrangement and condensation of the subunit hydrophobic core, suggested that periplasmic chaperones might trap subunits in a high-energy molten globule-like folding-intermediate state [8]. A model was proposed in which release of the subunit followed by DSC allows folding to be completed, driving fibre formation. However, previous studies have suggested a high value for the constant of association of the Caf1M–Caf1 chaperone–subunit complex (2×10^8 M^{-1}) [11], comparable with the equilibrium constant for folding of a stable globular protein. Despite numerous efforts, no quantitative equilibrium data on chaperone–subunit binding have been obtained in studies of other chaperone/usher systems. It was noticed, however, that complexes do not show significant dissociation, even in highly diluted solutions, which was taken as evidence of a very low dissociation constant [12]. It is hence not clear that the energy released on formation of the more compact fibre module would be sufficient to overcome the energy of chaperone–subunit binding.

In the present paper, we show that collapse of the subunit and final packing of its hydrophobic core is an essential component of the fibre assembly process. We show further that the chaperone–subunit complex is less stable than was previously thought, whereas the fibre module is exceptionally stable. The chaperone uses an extensive subunit-binding interface to bind and stabilize subunits in a high-energy conformation. This is accomplished by targeting unfolded subunit conformations and funnelling them into a unique activated conformation.

MATERIALS AND METHODS

Protein expression and purification

Expression and purification of Caf1M–Caf1 binary complex was performed as described previously [13]. pFM1-F1-6HSC, encoding only Caf1-SC (self-complemented subunit), was created by site-directed mutagenesis. Initially, the sequence encoding the complete G_d strand was inserted by two-stage asymmetric PCR [14] using pFM1′-F1-6H as a template and coding primer (inserted sequence in lower case) 5′-CCGTAACCGTATCTAACCAAgctgaccttacagcgtctactacggcgacagccaccttagtagagTAATCCATATAGATAATAG-3′. The short linker was then inserted using the standard mutagenesis protocol [15] and coding primer 5′-GTAACCGTATCTAACCAAaacggaGCTGACCTTACAGCGTCTACTAC-3′. Following induction of *Escherichia coli* DH5α/pFM1-F1-6HSC and periplasmic extraction, as described in [15], Caf1-SC was isolated by Ni^{2+}-affinity chromatography and was eluted with a gradient of 20–500 mM imidazole. Dialysed protein in 20 mM bis-Tris/propane, pH 7.1, was purified further by anion-exchange chromatography on Mono Q HR 5/5 columns (Amersham Biosciences, Uppsale, Sweden). Protein was eluted with a 0–250 mM NaCl gradient. Caf1M was purified from periplasmic extracts of *E. coli* B834 (DE3) cells transformed with pTCA1 by cation exchange on Mono S HR 10/10 columns (Amersham Biosciences) chromatography at pH 7.5. Surface fibres of F1 antigen were purified as described in [11]. Native Caf1M–$Caf1_2$ and Caf1M–$Caf1_3$ complexes were purified from periplasmic extracts of *E. coli* B834 (DE3) cells transformed with pFM1 [16] by anion- and cation-exchange chromatography on Mono Q HR 10/10 and Mono S HR 5/5 columns (Amersham Biosciences) at pH 7.5 and 4.5 respectively. Between these steps, samples were treated by TAGZyme exoproteolytic dipeptidase (Qiagen) to remove the free N-terminal donor sequence of the ultimate Caf1 subunit in the polymer.

X-ray crystallography

Crystallization of the Caf1M–$Caf1_2$ complex was performed as described previously for the A9R mutant ternary complex [13]. The crystals belong to space group $P2_12_12$ with unit cell dimensions $a = 180.1$ Å (1 Å = 0.1 nm), $b = 69.8$ Å and $c = 45.7$ Å, and one copy of the complex in the asymmetric unit.

Diffraction data ($\lambda = 1.01$ Å) were collected under liquid nitrogen cryoconditions at 100 K on a Marmosaic 225 CCD (charge-coupled device) detector at beamline BM14U, ESRF (European Synchrotron Radiation Facility), Grenoble, France. Data to 2.2 Å Bragg spacing were collected, processed and reduced using MOSFILM, and scaled using SCALA [17] (Table 1). The structure was solved by molecular replacement using AMoRe [18] with the A9R mutant ternary complex (Protein Data Bank accession code 1P5U) as a search model. Refinement was performed using the CNS program [19] (Table 1).

Microcalorimetry

Scanning microcalorimetry experiments were performed using a computer-driven version of the DASM-4 microcalorimeter [20] with a cell volume of 0.47 ml at a heating rate of 0.5–2 K/min. Protein concentrations in the calorimetric experiments varied from 0.5 to 10.8 mg/ml. Before experiments, protein samples were dialysed extensively against 20 mM phosphate buffer, pH 7.2, which was loaded into the reference capillary. The C_p (partial heat capacity of the protein) and the transition excess heat capacity function were calculated from the calorimetric data as described previously [20]. The protein partial specific volume was taken as 0.73 ml/g.

Lower limit values for the association constant for fibre module formation were estimated according to the procedure suggested by Brandts and Lin [21] for the case of binding with stoichiometry 1:1 and a single unfolding transition. Briefly, the enthalpy of unfolding for non-ligated (not complemented with the donor strand) subunit was estimated using the experimental value for the

Table 1 Data and refinement statistics

Values for high-resolution shells in parenthesis. $R_{merge} = \Sigma_h \Sigma_i |I(h)_i - \langle I \rangle| / \Sigma_h \Sigma_i I(h)_i$, where $I(h)$ is the intensity of a reflection h, Σ_h is the sum over all reflections and Σ_i is the sum over i measurements of reflection h. $R_{work} = \Sigma |F_O - F_C| / \Sigma F_O$ where F_O and F_C are the observed and calculated structure factors respectively. R_{free} is calculated for a test set of reflections randomly excluded from refinement. R.M.S.D. stereochemistry is the deviation from ideal values. R.M.S.D. B-factors is deviation between bonded atoms.

(a) Data collection ($\lambda = 1.01$ Å)

Parameter	Value
Resolution range (Å)	45–2.2 (2.32–2.2)
Number of unique reflections	28353 (4102)
Multiplicity	3.7 (3.6)
Completeness	94.6 (94.6)
R_{merge}	0.07 (0.22)
$\langle I/\sigma(I) \rangle$	7.6 (3.5)

(b) Refinement

Dataset	Native data
Resolution (Å)	20–2.2
Number of reflections	
Total	28353
Work set	26930
Test set	1423
R_{work}	0.223
R_{free}	0.244
Number of atoms	
Protein	3574
Solvent	229
Average B-factor (Å^2)	24.6
Solvent B-factor (Å^2)	28.9
R.M.S.D. stereochemistry	
Bonds (Å)	0.006
Angles (°)	1.36
R.M.S.D. B-factors (Å^2)	
Main chain	1.32
Side chain	2.16

free energy of unfolding of Caf1 at 25 °C ($\Delta G^{298K} = 8$–10 kJ/mol; V. M. Tischenko, unpublished work), the change of specific heat capacity (ΔC_p) for the fibre module, and an upper limit value for the melting temperature (T_0) (see the Discussion), according to the equation:

$$\Delta H(T_0) = [\Delta G^{298K} - \Delta C_p(298 - T_0) - T\Delta C_p \ln(T_0/298)]T_0/(T_0 - 298)$$

The constant of association of the complex (fibre module) at the experimental melting temperature (T_m) was estimated using a ligand (donor strand) concentration ($L_{tot/2}$) equal to half of the initial concentration of the complex according to the equation:

$$K_a(T_m) = \exp[-\Delta H(T_0)(1/T_m - 1/T_0)/R]\exp[\Delta C_p(\ln T_m/T_0 + T_0/T_m - 1)/R]/L_{tot/2}$$

The enthalpy of association and the association constant at temperature T were approximately estimated using the experimental value of the enthalpy of melting of the complex (ΔH^{cal}) according to the equations:

$$\Delta H_a = \Delta H(T_0) + \Delta C_p(T_m - T_0) - \Delta H^{cal}(T_m)$$
$$K_a(T) = K_a(T_m)\exp[-\Delta H_a(1/T - 1/T_m)/R]$$

Protein cross-linking

Cross-linking analysis of Caf1-SC was performed by incubating 1 mg/ml Caf1-SC in 50 mM phosphate buffer, pH 7.2, containing different concentrations of glutaraldehyde (0.02–2.5 %) for 0.5 h. The reaction was stopped by adding glycine, pH 8.0, and samples were analysed by SDS/PAGE (12.5 % polyacrylamide). Cross-linking of a tetramer of Caf1M was used as a positive control (results not shown).

CD

CD spectra for Caf1-SC were recorded on a J-810 dichrograph (Jasco) equipped with a PTC-423S temperature-control system (Jasco) in 0.1 cm path-length quartz cuvettes. Typically, five spectra recorded at a scanning speed of 50–100 nm/min with bandwidth set to 1 or 2 nm were accumulated.

MD (molecular dynamics)

Two 750 ps MD simulations were carried out with AMBER [22] using the Cornell et al. [23] force-field, one starting from the chaperone-bound (open) and one from the fibre (closed) conformation of Caf1. Both structures were placed in a 100 Å × 70 Å × 70 Å box and solvent (TIP3P [24]) was added to fill the remaining volume. Simulations were performed at 300 K using a time step of 2 fs, constant pressure and periodic boundary conditions. Long-range interactions beyond a 10 Å cut-off (updated every 25th MD step) were treated with PME (particle mesh Ewald) [25].

RESULTS

Complete collapse of the hydrophobic core is required for efficient assembly

The reported structure of the minimal *Y. pestis* F1-antigen fibre (Caf1′–Caf1″) capped by the Caf1M chaperone [8] reveals subunit conformation and interactions between subunits in F1 fibres. However, the complex used for structure determination was obtained by engineering a single amino acid substitution (A9R) in the N-terminal donor strand of the subunit, which effectively blocks the formation of larger fibres (Figure 2a). To understand the structural basis for the large difference in polymerization efficiency between this mutant and WT (wild-type) Caf1 subunit [16], native Caf1M–Caf1′–Caf1″ was purified from a mixture of complexes accumulating in the periplasm. Polymerization was blocked by enzymatic degradation of the flexible N-terminal donor sequence of Caf1″. Crystals of the native complex were grown in the same conditions as those of the mutant complex, and the structure was solved by molecular replacement using the mutant complex as a search model (Table 1).

The structures for Caf1M–Caf1′ in the WT and mutant Caf1M–Caf1′–Caf1″ ternary complexes (Figure 2b) are very similar, with an R.M.S.D. (root mean square deviation) of 0.259 Å for 330 aligned Cα positions, and the quaternary structures of the ternary complexes are virtually identical. Significant differences are found in the structure of the Caf1″ fibre subunit (Figure 2c). In both structures, the G_d donor strand of Caf1′ is inserted into the hydrophobic acceptor cleft of Caf1″. In the mutant complex, the engineered Arg^9 side chain in the G_d donor strand is in a bent conformation with the guanidinium group pointing into solution. The Cβ and Cγ atoms are directed towards the hydrophobic cleft and pack between the two sheets of the subunit β-sandwich [8]. The smaller alanine side chain in the native donor strand relaxes these contacts, allowing full contact between the two sheets. Hence, condensation of the hydrophobic core reaches completion

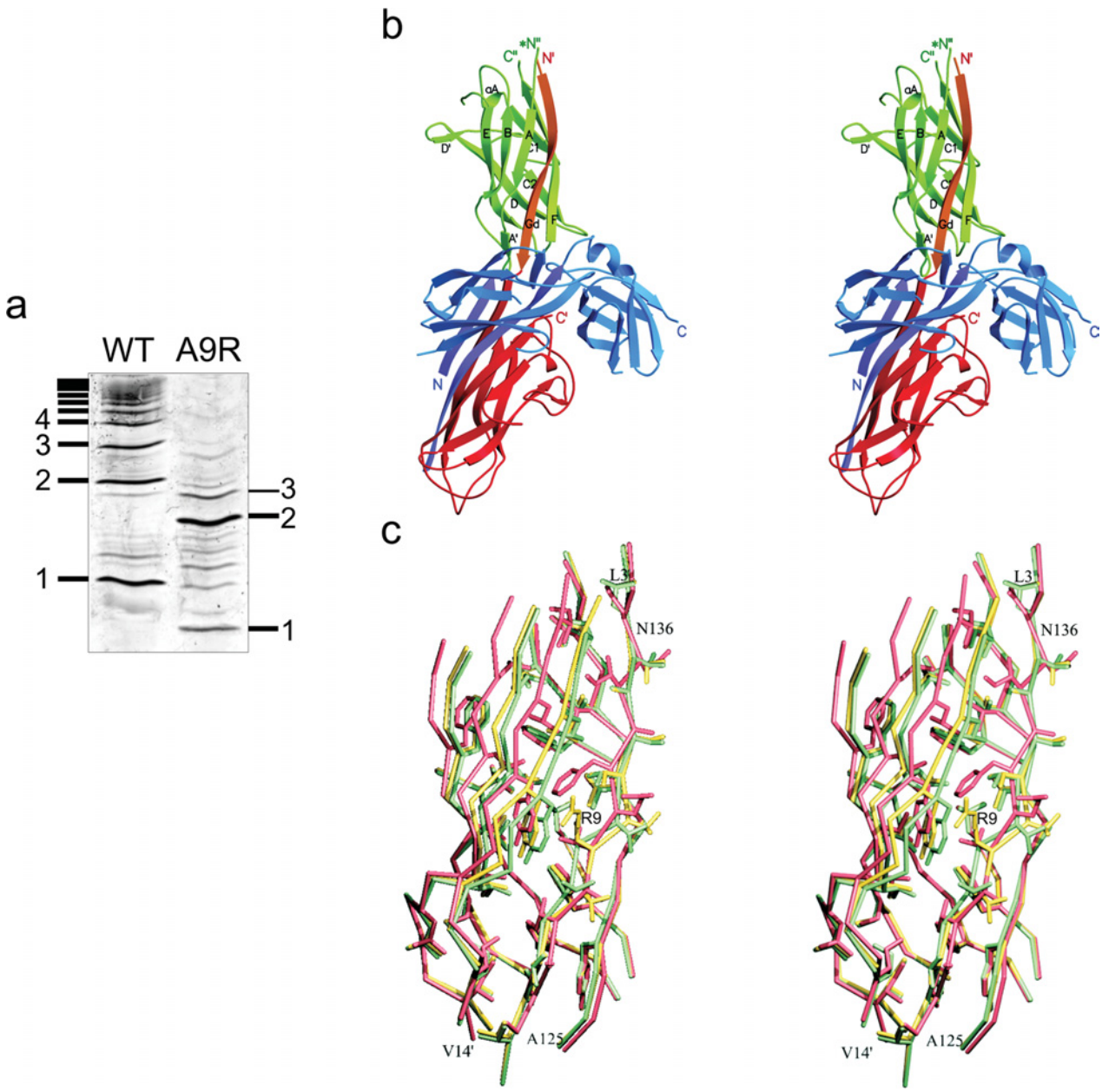

Figure 2 Comparison of WT and A9R Caf1M–Caf1′–Caf1′′ complexes

(**a**) IEF of native (left-hand lane) and mutant (right-hand lane) Caf1M–(Caf1)$_n$ complexes accumulating in the periplasm of cells lacking the usher export channel. Bars show positions of bands of complexes with the indicated number of subunits. Most of these species have been characterized thoroughly, and structures are available for ternary and binary complexes [8,13,16]. The level of secretion of the mutant protein was lower than that of the native one in this experiment. (**b**) Stereo diagram of the native Caf1M–Caf1′–Caf1′′ complex. Caf1M is in blue, except for G_1 and A_1 β-strands (violet). The chaperone-bound Caf1′ subunit is red [N-terminal donor strand (G_d) is orange]; the Caf1′′ subunit corresponding to the tip of a growing fibre is green. N- and C-termini are labelled in the same colours as the ribbons. The asterisk in the *N′′ label indicates that the N-terminal sequence of Caf1′′ up to this point is removed. (**c**) High-resolution 'snap-shots' of subunit collapse upon donor strand exchange. Caf1′, Caf1′′ A9R and Caf1′′ WT are red, yellow and green respectively (stereo view). Complementing donor strands are shown in the same colours as the complemented subunits. To avoid clutter, only β-strands in the two sheets of each subunit are shown. Ala^{125} and Asn^{136} of the chaperone G_1 as well as Leu$^{3'}$ and Val$^{14'}$ of the subunit G_d donor strands and Arg^9 of Caf1′′ A9R are labelled.

in the native structure, whereas the A9R mutant is trapped in an intermediate state. This result suggests that complete collapse of the subunit hydrophobic core is required for efficient fibre assembly.

Thermodynamics of Caf1 subunit before and after assembly

Our model for fibre assembly states that the process is thermodynamically driven by energy released on collapse of the subunit hydrophobic core [8]. Blocking complete collapse as in the A9R mutant would then be expected to impede assembly by reducing the amount of energy available for release. However, the apparent stability of chaperone–subunit complexes ($K_a = 2 \times 10^8$ M^{-1}) [11] implies that final folding of subunit and formation of fibre module would have to release an exceptional amount of free energy in order to be able to drive assembly. We therefore decided to investigate the energetics of the system by direct measurement of thermodynamic parameters for the relevant pre- and

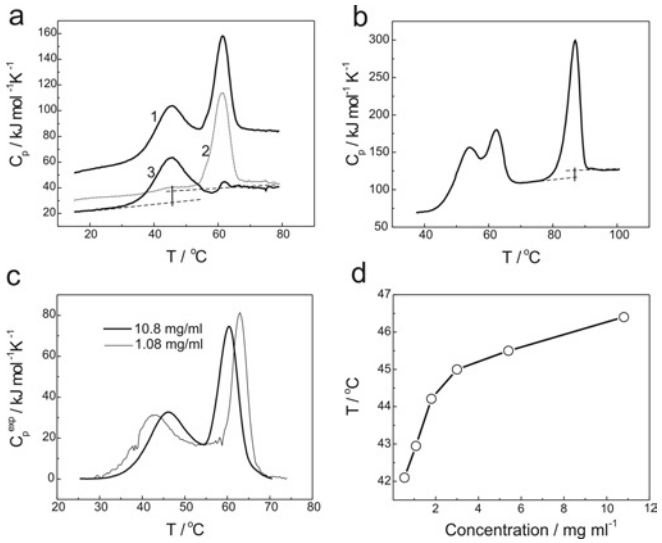

Figure 3 Thermal denaturation of Caf1M–Caf1 and Caf1M–Caf1$_2$ complexes observed by differential scanning calorimetry

(**a**) Molar heat capacity curves for Caf1M–Caf1 at 3 mg/ml (1), Caf1M at 2.5 mg/ml (2) and (1)−(2) difference curve (3). (**b**) Molar heat capacity curve for Caf1M–Caf1$_2$ (2.2 mg/ml). (**c**) Transition excess heat capacity curves for Caf1M–Caf1 at 1.08 and 10.8 mg/ml. (**d**) Dependence of the T_m of Caf1M–Caf1 at the peak maximum on the concentration. Broken lines in (**a**) and (**b**) show linear extrapolation of pre- and post-transitional dependences to the transition area.

post-assembly states of the subunit (in complex with the chaperone, and in fibres).

Efforts to characterize chaperone–subunit binding quantitatively with equilibrium assays have been thwarted by problems of subunit aggregation [12,26]. Aggregation problems make the study of subunit–subunit interactions using equilibrium methods even more intractable. We therefore chose to characterize bound states of the subunit using differential scanning microcalorimetry (Figures 3, 4 and 5; Table 2), which provides a direct measure of thermodynamic parameters. Microcalorimetric data for protein complexes can in favourable cases be interpreted in terms of binding and folding equilibrium constants [21,27]. To prevent polymerization processes from interfering with the calorimetry measurements, complexes where the free N-terminal donor strand of the tip-located Caf1 subunit had been removed either genetically or enzymatically were used in all experiments.

Two heat absorption peaks with maxima at 45 and 62 °C are observed in the molar heat capacity curve of the Caf1M–Caf1 (binary) complex (Figure 3a, curve 1; 3 mg/ml). The second peak of the curve (55–70 °C) is similar to the single transition in the melting curve for free Caf1M (Figure 3a, curve 2). The observed transition temperature ($T_m = 61.5$ °C) is close to that determined previously for Caf1M using spectroscopic methods [11]. These data suggest that the second peak in the molar heat capacity curve of the binary complex is due to melting of the chaperone. Hence, the first transition most likely is caused by melting of Caf1 accompanied by complex dissociation to unfolded Caf1 and native Caf1M. This transition partially overlaps with the melting of Caf1M, but can be isolated by the subtraction of melting curve 2 from curve 1 (curve 3). Figure 4(a) shows the transition excess heat capacity curves for Caf1M–Caf1 and Caf1M obtained by subtraction of the intrinsic heat capacity from the experimental curves. The intrinsic heat capacity was modelled by extrapolating the pre- and post-transitional heat capacities into the transition zone in proportion to the progress of heat absorption as described in [20].

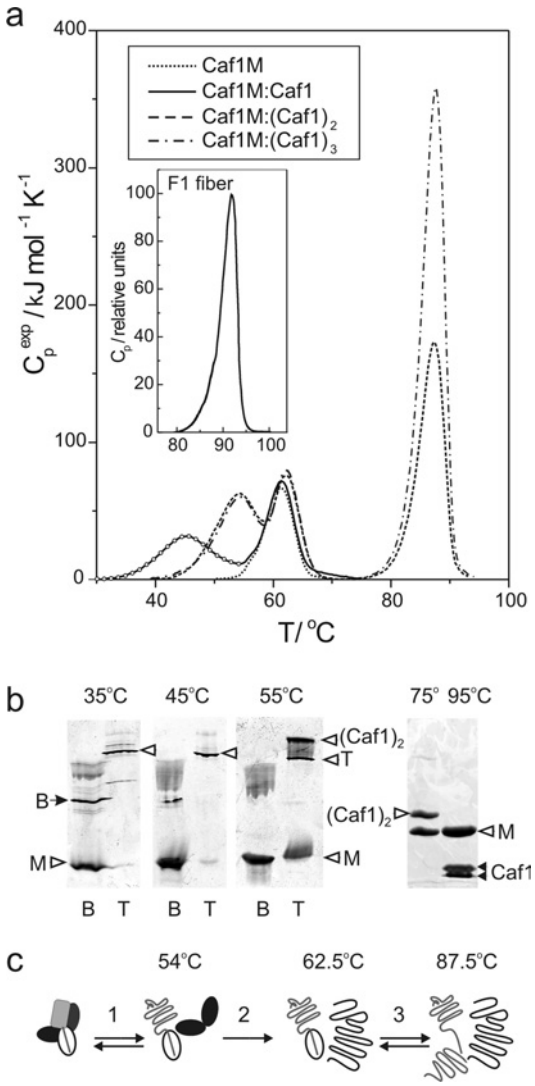

Figure 4 Chaperone traps a high-energy folding intermediate of the subunit

(**a**) The transition excess heat capacity of Caf1M (· · · · ·), Caf1M–Caf1 (—; ○ indicates fully reversible transition), Caf1M–Caf1$_2$ (– –), and Caf1M–Caf1$_3$ (– · – · –). The N-terminal donor strand of the subunit in Caf1M–Caf1 has been removed genetically and the free donor strand at the tip of Caf1M–Caf1$_2$ and Caf1M–Caf1$_3$ complexes has been removed enzymatically as described in the Materials and methods section. Complexes were studied at approximately equal concentrations (40–70 μM) to allow proper comparisons. The inset shows the excess heat capacity curve for F1 fibres isolated from the cell surface. (**b**) IEF of Caf1M–Caf1 and Caf1M–Caf1$_2$ on pH 3–9 gels (5 % polyacrylamide) at the indicated temperatures (left-hand panels). SDS/PAGE (12.5 % polyacrylamide) of Caf1M–Caf1$_2$ pre-heated at 75 and 95 °C (right-hand panel). Arrowheads at B, T and M indicate positions of focusing of the binary (Caf1M–Caf1) and ternary (Caf1M–Caf1$_2$) complexes, and free Caf1M respectively. Arrowheads at Caf1$_2$, Caf1 and M indicate bands of Caf1 dimer, Caf1 denatured monomer (with intact (upper band) and digested (low band) N-terminal donor sequence) and Caf1M respectively. (**c**) Scheme illustrating the sequential process of melting of Caf1M–Caf1$_2$. Black, Caf1M; grey, Caf1′; white, Caf1″. The donor strand of Caf1′ complementing Caf1″ is shown as a thin black line. The donor strand sequence of Caf1″ was enzymatically removed to block further polymerization (and therefore not shown).

IEF (isoelectric focusing) of the binary complex was performed at different temperatures on 5 % gels (Figure 4b, lanes B). The complex is focused in a single band of pH 6.2 at room temperature (20 °C). The band starts to disappear as the temperature approaches 35 °C and vanishes completely at 55 °C. At the same time, free chaperone molecules (band at pH 8.2) and subunits (a smear around pH 5.5, typical for denatured proteins) accumulate. These

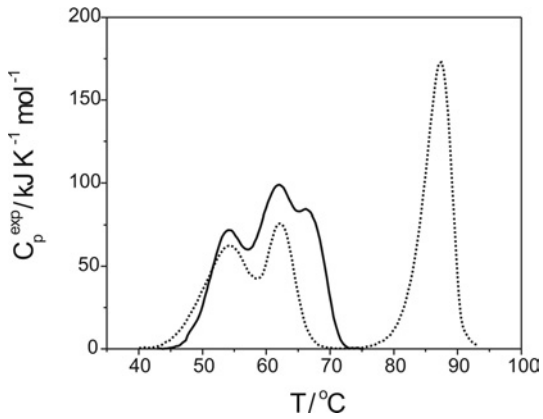

Figure 5 Complete collapse of the subunit hydrophobic core is essential for achieving stable fibre module

The transition excess heat capacity curves of the native (dotted line) and A9R mutant (solid line) Caf1M–Caf1$_2$ complexes.

Table 2 Thermodynamic parameters of melting of Caf1M and Ca1M–Caf1 complexes

Results were calculated form the three best thermograms selected from all melting experiments (different concentrations of samples). S.D. and number of independent experiments are indicated.

Sample	Transition	T_m (°C)	ΔH^{cal} (kJ/mol)	$^*\Delta C_p$, kJ/mol/K
Caf1M (2.5 mg/ml)		61.5 ± 0.5 (4)	415 ± 25 (4)	
Caf1M–Caf1 (3 mg/ml)	1	45.1 ± 0.4 (4)	355 ± 30 (4)	10.1 ± 1.0 (3)
	2	61.7 ± 0.4 (4)		
Caf1M–Caf1$_2$ (2.2 mg/ml)	1	54.2 ± 0.7 (3)	505 ± 35 (3)	
	2	62.4 ± 0.5 (3)		
	3	87.5 ± 0.5 (3)	840 ± 50 (3)	8.8 ± 1.3 (3)
Caf1M–Caf1$_3$ (2 mg/ml)	1	53.9, 54.3	511, 540	
	2	62.7 ± 0.6 (3)		
	3	87.8 ± 0.5 (3)	1790 ± 70 (3)	

observations are consistent with a temperature-induced dissociation of the complex into a free chaperone molecule and a denatured subunit. This process correlates with the first heat absorption peak in the melting curve for the binary complex. The results support the idea that this peak corresponds to the melting of Caf1, and that melting occurs simultaneously with dissociation of the complex. The first transition in the excess heat capacity curve of the binary complex is fully reversible (Figure 4a), as judged by a nearly perfect overlap of repeating scans. Changes of the scan rate in the range 0.5–2 °C/min practically did not affect the temperature and shape of this transition (results not shown). This result suggests complete and relatively fast re-folding of Caf1 upon rebinding.

Melting experiments performed at different concentrations of the complex detected shifts of the peak maximum temperature from 42.1 to 46.5 °C, with a change of the concentration from 0.5 to 10.8 mg/ml (Figures 3c and 3d). The observed concentration dependence proves that the denaturation of Caf1 and dissociation of the complex are coupled processes [28]. Surprisingly, the melting temperature of the second peak was also concentration-dependent. However, in this case, T_m decreased with increasing concentration. Melting experiments with the chaperone alone revealed a similar effect. We believe that this concentration effect is caused by an association of denatured Caf1M molecules into oligomeric structures, providing an apparent stabilization to the denatured conformation and shifting the equilibrium towards denaturation. This secondary process would also explain the observed poor reversibility of the transition and the asymmetry of the peak.

Three heat absorption peaks with maxima at 54 °C, 62.5 °C and 87.5 °C are observed in the molar heat capacity curve for the WT Caf1M–Caf1′–Caf1″ (ternary) complex (Figure 3b). The transition excess heat capacity curve obtained from this diagram is shown in Figure 4(a). IEF of the ternary complex (Figure 4b, lanes T) reveals a single band (pH 5.1) that gradually disappears at temperatures corresponding to peak 1 (45–60 °C). Chaperone (pH 8.2) and subunit (pH 4.5) bands accumulate instead. This is similar to dissociation of the binary complex. SDS/PAGE (12.5 % polyacrylamide) of the sample pre-heated at 75 °C (Figure 4b, right-hand panel) resulted in two bands with molecular masses of those of Caf1M (27 kDa) and Caf1′–Caf1″ (30 kDa, N-terminal sequence is absent from Caf1″), suggesting that Caf1′–Caf1″ is the product released at the first denaturation event.

Since the chaperone-bound subunit Caf1′ is released and undergoes denaturation at the first transition, inter-subunit DSC is likely to be the major contact linking subunits in Caf1′–Caf1″. SDS/PAGE (12.5 % polyacrylamide) of the ternary complex pre-heated to 95 °C displays three bands corresponding to chaperone and two species of denatured subunits, one (Caf1′) with intact (upper, 15.5 kDa) and the other (Caf1″) with truncated (lower, 14.5 kDa) N-terminal sequences. The results imply that the fibre module consisting of donor-strand-complemented Caf1″ denatures somewhere between 75 and 95 °C. Indeed, melting/dissociation of Caf1′–Caf1″ results in an impressive heat absorption peak within the 80–95 °C temperature interval (Figure 4a). This peak occurs at the same temperature as the single transition observed for melting of full-length F1 antigen purified from the surface of bacteria (Figure 4a, inset). The excess heat capacity curve for the Caf1M–(Caf1)$_3$ (quaternary) complex (Figure 4a) essentially repeats that for the ternary complex. The larger size of the third peak is expected, since the dissociated Caf1$_3$ polymer contains two, rather than one, fibre modules. The melting process of the ternary complex suggested by the data is summarized schematically in Figure 4(c).

Melting of the minimal polymer generates a large peak in the heat capacity curve ($T_m = 87.5$ °C and $\Delta H^{cal} = 840 \pm 50$ kJ/mol, 2.2 mg/ml; Figures 3b and 4a). The presence of a single peak at rather high temperatures suggests a highly stable co-operative structure for the donor-strand-complemented fibre module Caf1″. The temperature of the peak maximum depends on the concentration of the complex, shifting by ~2 °C with a change of the concentration from 0.5 to 5 mg/ml (results not shown). The lower concentration-dependence for this peak than for the dissociation/denaturation of Caf1′ observed in experiments with binary complex is expected because of the high enthalpy change of the transition [28].

Coupled release and unfolding of Caf1′ from the binary pre-assembly complex occurs at $T_m = 45$ °C with an enthalpy of $\Delta H^{cal} = 355 \pm 30$ kJ/mol (3 mg/ml). Linear extrapolation of the pre- and post-transitional heat capacities to the mid-temperature of the transition peaks (Figure 3a, curve 3 and 3b, peak 3) gives direct estimates for the partial molar heat capacity change for dissociation/denaturation of pre-assembly complex Caf1′ and fibre Caf1″ of $\Delta C_p = 10.1 \pm 1.0$ and 8.8 ± 1.3 kJ/mol per K respectively. Assuming that the partial molar heat capacity changes do not depend significantly on temperature, enthalpies for dissociation/denaturation of Caf1′ and Caf1″ can be estimated at different temperatures using the equation $\Delta H(T) = \Delta H(T_m) + \Delta C_p(T - T_m)$, where T_m and $\Delta H(T_m)$ are the experimentally determined temperature and enthalpy of melting. This allows comparison of the

enthalpies at the same temperature. For example, the dissociation/denaturation enthalpy at 37 °C for Caf1′ in the binary complex is estimated to be approx. ~275 kJ/mol, whereas the enthalpy for Caf1″ at this temperature is estimated to be ~395 kJ/mol. Hence, Caf1′ and Caf1″ exhibit large differences in thermostability ($\Delta T_m = 42.5$ °C) and enthalpies of melting.

Compared with the binary complex, chaperone dissociation and Caf1′ unfolding occurs significantly later in the thermograms for the ternary and quaternary complexes, suggesting a significantly higher stability of Caf1′ in these complexes. This is explained by the presence of a neighbouring Caf1″ fibre module that stabilizes Caf1′ and by the additional interactions between polymeric Caf1 and Caf1M [8]. The total enthalpy of the region of peaks 1 and 2 in the thermograms is a sum of enthalpies of melting of Caf1′ in the complex, the contact between Caf1M and Caf1″, and Caf1M itself. Subtraction of the enthalpy for Caf1M from this value yields the enthalpy of melting of Caf1′ in the ternary complex (including melting of the contact between Caf1M and Caf1″), which is estimated at 505 ± 35 kJ/mol ($T_m = 54$ °C). This is larger then the enthalpy of melting of Caf1′ in the binary complex (~445 kJ/mol), but again smaller than the enthalpy of melting of Caf1″ (~545 kJ/mol) at this temperature. The difference between the enthalpies of melting of Caf1′ and Caf1″ in the ternary complex is expected to be higher at physiological temperatures.

Melting of the A9R ternary complex (Figure 5) also results in three peaks in the excess heat capacity curve, with maxima at approx. 55 °C, 63 °C and 65–70 °C. The first two transitions, corresponding to melting of Caf1′ and of Caf1M respectively, occur at the same temperature and with essentially the same enthalpy as in the WT ternary complex. However, the third transition (evident as a shoulder on the curve), corresponding to melting of the fibre module, occurs at a dramatically lower temperature and with much less release of heat than observed for the WT fibre module. This result confirms that blocking of subunit collapse by insertion of a large non-native donor side chain in the acceptor cleft significantly destabilizes the donor-strand-complemented module and explains the poor assembly efficiency of A9R Caf1.

Caf1-SC folds into a highly stable monomeric structure

Although the minimal fibre is a simple and reliable model for the study of fibre assembly, quantitative biophysical characterization using this construct is still problematic. In search for a simpler model, a circularly permuted self-complemented subunit [29,30] (Caf1-SC) was constructed. Caf1-SC contains the donor sequence fused at the C-terminus, rather than at the N-terminus, which allows insertion of this self-complementing G_d strand in the acceptor cleft, restoring a classical Ig-fold [29,30]. Thus a single-chain fibre module was obtained, for which both unfolding and folding are first-order processes, making it easier to investigate. The donor sequence was linked to the C-terminus via a Asn-Gly duplet in order to optimize the β-turn between the F_1 and G_1 strands, creating the C-terminal sequence QNGADLTASTTATATLVE. A His_6 tag replaced the native N-terminal G_d extension, allowing purification of the subunit from the periplasm.

Caf1-SC accumulates as a monomer according to analysis by analytical gel filtration and glutaraldehyde cross-linking (Figure 6a). Caf1-SC displays a far-UV CD spectrum similar to that of F1 surface fibres [31], but with a higher intensity at the minimum (-2000 deg · cm^2 · dmol^{-1} at 208–209 nm), which makes it more 'typical' for β-structural proteins (Figures 6b and 6d). The spectrum becomes gradually more negative with heating up to 75–80 °C (Figures 6b and 6c). Further heating (80–90 °C) induces a sharp change with maximum amplitudes at 217–224 nm and below 210 nm, reflecting protein denaturation. The transition is basically reversible as judged by essential recovery of the native spectrum after cooling of samples. Two-state model analysis of the transition as monitored by the ellipticity at 220 nm reveals a T_m of 85.5 °C and a van't Hoff enthalpy, ΔH^{vH}, of 810 ± 60 kJ/mol (Figure 6c, inset).

CD analysis of Caf1-SC in GdmCl (guanidium chloride)-containing solutions (up to 6.5 M) at 20 °C (Figure 6d) and 43 °C (results not shown) does not reveal any significant spectral changes to suggest large changes in structure. Resistance to such strong denaturing conditions suggests an unusually high stability of the protein. At 55 °C, however, a co-operative transition is observed within 3.75–5 M GdmCl (Figures 6e and 6f). The maximum changes are observed at 220–225 nm and below 212 nm, as in the case of temperature denaturation. However, owing to the noise level at high concentrations of GdmCl, only the 220–225 nm region was chosen for analysis of the transition. The transition is sufficiently reversible (more than 80 %) to apply two-state equilibrium analysis (Figure 6f). Estimation of the free energy of unfolding according to the procedure of Santoro and Bolen [32] yields $\Delta G^{55\,°C} = 55.6 \pm 3.0$ kJ/mol and a co-operativity of 13.2 ± 0.7 kJ/mol per M.

MD simulations predict spontaneous collapse of the chaperone-bound subunit conformation

The chaperone-bound conformation, although native-like, is predicted to be highly unstable in solution owing to the poor packing of its β-sheets [8]. Our data for melting of the A9R fibre module demonstrates that insertion of large non-native residues in the acceptor cleft has a destabilizing effect. Our microcalorimetry data argue that the chaperone–subunit complex is not very stable, in spite of an extensive and well-packed interface [8]. Taken together, these data strongly suggest that the chaperone-bound conformation corresponds to an unstable high-energy state. To investigate this further, we carried out MD simulations starting from both the chaperone-bound (Caf1′, open) and fibre (Caf1″, closed) structures of Caf1. Simulations starting from the closed structure resulted in little change, other than in the surface-exposed loop regions. Structural analysis of the most populated conformations observed in simulations starting from the open conformation reveals that the simulation converges to a structure that is more similar to the fibre conformation (R.M.S.D. 1.7 Å for 132 Cα positions) than to the open one (R.M.S.D. 2.0 Å for 132 Cα positions). The packing and the fit between the two sheets of the subunit β-sandwich improve in the simulation, as reflected in an increase of the shape correlation statistic S_c [33] from 0.58 in the open starting conformation, to 0.64 at the end of the simulation. Hence, the simulations predict that the open conformation tends to spontaneously collapse into a more compact, closed, conformation.

DISCUSSION

Collapse of the subunit into a highly stable structure drives fibre formation

Comparison of the structures for mutant (A9R Caf1) and WT ternary complexes (Figure 2c) shows that condensation of the hydrophobic core reaches completion only in the native structure, explaining the lower assembly efficiency of mutant fibres (Figure 2a). Whereas the incomplete collapse observed in the mutant complex is already sufficient for the formation of assembly-initiating minimal fibres, it is only the perfect packing of the core obtained in the WT complex that allows the elongation process to produce full-length organelles. A significant stabilizing

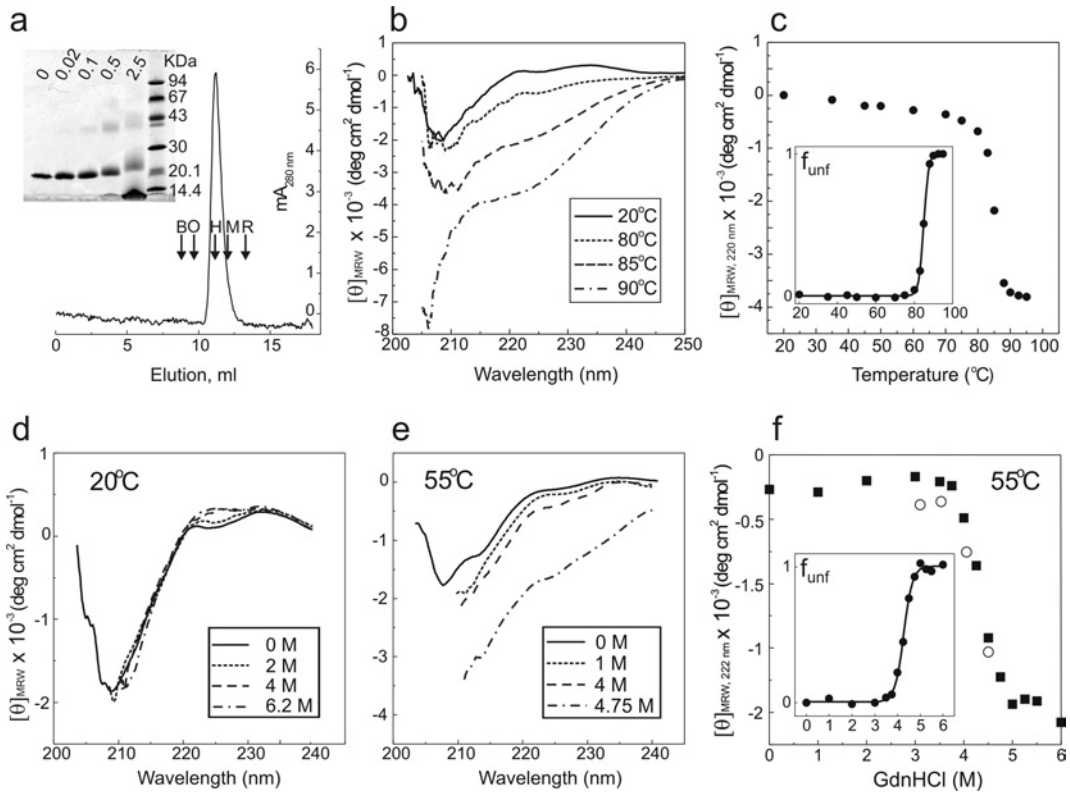

Figure 6 Self-complemented subunit folds into a highly stable structure

(**a**) Caf1-SC accumulates as a monomer in the periplasm. Elution profile of Caf1-SC loaded on a Superdex 75 HR 10/30 gel filtration column. Elution volumes for the marker proteins are indicated by arrows. B, BSA; O, ovalbumin; H, chymotrypsinogen A; M, myoglobin; R, ribonuclease A. Analysis of the selectivity curve (not shown) yields an apparent molecular mass for Caf1-SC of 23.5 kDa. The inset shows Coomassie-Blue-stained SDS/PAGE (12.5% polyacrylamide) of Caf1-SC samples pre-incubated in phosphate buffer containing different concentrations of glutaraldehyde (%). No specific cross-linking is observed. Molecular-mass sizes are given in kDa. (**b**) Far-UV CD spectra of Caf1-SC at different temperatures. (**c**) Temperature-dependence of ellipticity at 220 nm. Fraction of unfolded protein is shown in the inset. (**d**) and (**e**) Far-UV CD spectra of Caf1-SC samples containing different concentrations of GdmCl at 20°C (**d**) and at 55°C (**e**). Far-UV parts of spectra where the noise level was high (depending on concentration of GdmCl) are not shown. However, it was checked by multiple scans that spectra shown in (**d**) do not deviate more than $\pm$250 deg · cm^2 · dmol^{-1} from that recorded at 0 M GdmCl in the region 206–212 nm. (**f**) GdmCl-induced equilibrium transition at 55°C monitored by measurement of ellipticity at 222 nm. ■, unfolding; ○, refolding by dilution with GdmCl-free buffer. Fraction of unfolded sample is shown in the inset. Refolding data were not used in calculations. Measurements shown in (**b**) and (**c**) were performed at a protein concentration of 0.76 mg/ml in 10 mM phosphate buffer, pH 7.1, containing 75 mM NaCl. Measurements shown in (**d**), (**e**) and (**f**) were performed at protein concentrations of 0.3–0.6 mg/ml in 10 mM bis-Tris/propane buffer, pH 7.1, containing 50 mM NaCl.

contribution from the final fine packing of the subunit hydrophobic core is suggested by the melting of the A9R mutant ternary complex (Figure 5). The structurally observed incomplete collapse of the fibre subunit in this complex results in a dramatic decrease in the enthalpy and transition temperature for the melting of the fibre module (peak 3). These results provide strong evidence for our hypothesis that collapse of the subunit hydrophobic core shifts the equilibrium towards formation of fibres. However, in view of the large interface between chaperone and subunit in the pre-assembly complex, and the reported stability of this complex [11], spontaneous fibre assembly would not seem possible. We investigated this apparent paradox by thermodynamic analyses of pre- and post-assembly states of the Caf1 subunit.

Biochemical analysis of Caf1M–Caf1 and Caf1M–Caf1$_2$ complexes at different temperatures suggested that melting of Caf1 in the chaperone–subunit complex (Caf1′) and fibre module (Caf1″) occurs simultaneously with dissociation of the complex and module (Figure 4). The thermal unfolding of Caf1′ and Caf1″ observed by differential scanning calorimetry displays concentration-dependence, again suggesting that denaturation and dissociation are coupled processes. Both transitions are evident as single peaks with a slightly asymmetric shape typical for a two-state bimolecular denaturation (Figures 3 and 4).

Caf1′ and Caf1″ exhibit large differences in thermostability and enthalpies of melting (Figure 4 and Table 2). At concentrations of 40–70 μM, the difference in melting temperature of these forms is approx. 42.5°C. Tight binding to macromolecules, ligands and ions provides thermodynamic stabilization of the native conformation of proteins, which is reflected in an increased melting temperature [21]. Our structures show that DSC in pre-assembly complexes and in fibres stabilizes subunit conformations that differ significantly (Figure 2c). The dramatically higher melting temperature of Caf1″ indicates more efficient stabilization of the close-packed fibre conformation. The ΔC_p for denaturation/dissociation of both Caf1′ and Caf1″ (Figure 3 and Table 2) is relatively high ($\sim$0.62 and 0.56 J/g per K), suggesting large changes in the exposed hydrophobic surface area during the denaturation/dissociation process. The higher ΔC_p for Caf1′ may reflect the larger hydrophobic contact area between Caf1′ and Caf1M than between subunits in the fibre. At 37°C, Caf1″ exhibits a 1.5-times higher enthalpy of melting than Caf1′, indicating that the more close-packed Caf1″ fibre conformation is also better packed and more stable. The very high enthalpy of melting observed for Caf1″ (Table 2) is close to the maximum observed for globular proteins [34]. The dramatic differences between Caf1′ and Caf1″ in thermostability and enthalpies of unfolding/dissociation

suggest a large difference in thermodynamic stability between these forms [21].

Since the ratio of the calorimetric enthalpies obtained from peak 3 for the ternary and quaternary (Table 2) complexes is very close to 2, it is reasonable to assume that neighbouring fibre modules in the polymer denature essentially independently. Hence, denaturation of F1 fibre can be treated as approximately a two-state process of melting and dissociation of fibre modules. Estimation of a lower limit value for the association constant for subunit–subunit DSC (see the Materials and methods section), setting $\Delta C_p = \Delta C_{p,fibre}$, and $T_0 = T_{m,binary}$ (because the melting temperature of free subunit cannot exceed the melting temperature of binary complex), suggests that the binding constant at physiological temperatures is at least 10^{14} M^{-1}, rating DSC as one of the tightest known protein–protein and protein–ligand interactions [21].

In order to obtain a model for the fibre module that would lend itself to quantitative thermodynamic analyses, a Caf1-SC subunit was constructed. Temperature and GdmCl-induced denaturation of the resulting monomeric protein was monitored using CD (Figures 6b–6f). Two-state model analysis of the temperature-induced transition reveals a T_m of 85.5 °C and a ΔH^{vH} of 810 ± 60 kJ/mol. These values are similar to the parameters obtained calorimetrically from minimal fibres. However, even larger values might have been expected, since the covalent attachment of the donor strand increases the apparent concentration of the interacting components. The lack of such an effect might be explained by the presence of distortions in the structure introduced by the engineered connection of the G_d strand, and/or possibly by the additional subunit–subunit contacts present in fibres in addition to DSC [8]. Reversible GdmCl-induced unfolding at 55 °C allowed estimation of the free energy of unfolding, yielding $\Delta G^{55^\circ C} = 55.6 \pm 3.0$ kJ/mol and a co-operativity of 13.2 ± 0.7 kJ/mol per M. This value for the unfolding free energy at 55 °C is in the typical range for very stable globular proteins at 5–35 °C (the optimum stability range for most globular proteins) [34]. Extrapolation to physiological temperature (37 °C) using $\Delta G^{55^\circ C} = 55.6 \pm 3.0$ kJ/mol, $\Delta H^{vH} = 810 \pm 60$ kJ/mol and $\Delta G^{85.5^\circ C} = 0$ kJ/mol gives $\Delta G^{37^\circ C}$ in the region of 70–80 kJ/mol and ΔC_p of 8–11.5 kJ/mol per K. It might be that the apparently narrow range of optimal stability for globular proteins is explained by adaptation to physiological constraints, such as the need for protein turnover. In the case of assembly of pathogenic surface fibres, there is no pressure of this kind, which may explain the exceptional stability of fibre modules.

Explicit estimation of the association constant for chaperone–subunit DSC from the calorimetric data according to the standard procedure [21] is not possible because of the lack of experimental data on the melting of free subunit. However, the fact that the difference between the melting temperature of the pre-assembly complex (45 °C) and the physiological temperature of F1-antigen assembly (37 °C) is only 8 °C suggests that high thermodynamic stability of this complex at physiological temperatures is improbable.

Whereas the constant of dissociation of the Caf1M–Caf1 pre-assembly complex has proven difficult to obtain experimentally, the constant of association of chaperone and purified F1 fibres was determined successfully [11]. This association constant characterizes capping of fibres (including the minimal one) by the chaperone. The observed differences in the temperatures (9 °C) and enthalpies of dissociation/denaturation (~60 kJ/mol at 54 °C) of Caf1′ in minimal fibre and in pre-assembly complex suggests that capping of a single subunit is significantly weaker than capping of fibres, i.e. the association constant for the binary complex is expected to be significantly lower than the 2×10^8 M^{-1} measured for fibre capping [11]. Tighter fibre capping might be important for anchoring fibres in the outer membrane. However, it is easy to see that this does not influence the driving energy for fibre formation, because stoichiometric amounts of fibre-capping chaperones are among both reagents and products of the reaction (once the growing fibre contains two or more subunits). Thus our experiments suggest that the stability of the pre-assembly complex is lower than was previously thought, whereas the fibre module is unusually stable. This difference in stabilities creates a free energy potential that drives fibre formation.

The chaperone-bound subunit is trapped in an activated high-energy conformation

Thermodynamic stability of different forms of the Caf1 subunit appeared to correlate with the extent of contact between the two β-sheets of the subunit β-sandwich and thus on the degree of condensation of the core: Caf1′ and A9R Caf1″ with more expanded cores are energetically much less stable than native Caf1″ with the close packed core. This situation is similar to that observed for 'small-to-large' mutations in the hydrophobic core of T4-lysozyme, which tend to destabilize the protein [35].

The MD simulations show a strong tendency for the open conformation to adopt a closed fibre-like structure, suggesting that the chaperone traps a high-energy folding intermediate. The extensive hydrophobic interactions between the chaperone and subunit may compensate for this non-optimal conformation. Nonetheless, as shown here, the net stability of the binary complex, being a result of balancing the effects of instability of the bound activated subunit and binding, is relatively low. The apparent stability of the complex in diluted solutions over long incubation times (allowing high-yield purification of the complex) might be explained by the presence of a significant energy barrier for complex dissociation, which is reasonable to expect, since the open Caf1 structure must be released to solvent before it can collapse into an energetically more stable conformation. At the same time, this would provide a catalysable step along the assembly pathway, thereby allowing spatial and temporal control over the assembly process.

Several observations suggest that periplasmic chaperones target and bind subunits in an unfolded or at least partially unfolded state. The high efficiency of chaperone/usher-mediated assembly *in vivo* [10] suggests that this process cannot rely on the slow self-folding of subunits [26], which would be predicted to be accompanied by massive non-productive aggregation in the crowded environment of the periplasm. This was indeed observed experimentally in cells lacking the periplasmic chaperone [36]. Hence, folding is most likely assisted by the chaperone. Very recently, Vetsch et al. [37] verified that the FimC chaperone involved in assembly of type 1 pili indeed binds to unfolded pilin subunits. Chaperone binding was shown to increase the rate of folding by a factor of 100.

To achieve binding of unfolded subunits, the chaperone has to recognize a common feature of the (partially) unfolded conformations. The extensive hydrophobic interactions between the cores of the N-terminal domain of the chaperone and the subunit observed in the structures of complexes [5–8] suggests that the chaperone might recognize and attract hydrophobic core residues that are exposed in unfolded subunits, possibly a folding nucleus. Donor strand residues inserted by the chaperone into the acceptor cleft of the subunit are considerably larger than native residues in the G_d strand of the subunit [8]. The surface-exposed hydrophobic patch created by the bulky hydrophobic side chains in the donor strand of free chaperone [9,38] might attract (partially) unfolded subunits and provide a template on to which the subunit core can condense, facilitating folding. At the same time, however, the subunit is trapped in the open, activated, conformation because of

intercalation of the large non-native donor residues in the acceptor cleft. The resulting meta-stable complex provides a convenient substrate for assembly.

We thank Sergey Potekhin for advice on the theoretical treatment of the microcalorimetry results, and Gail Hutchinson for advice on β-turn optimization. This work was supported by a Wenner-Gren Foundations stipend (to A.V.Z.), by grant 03-04-48882 from the Russian Foundation for Basic Research (to V.M.T.), by grants from the Swedish Research Council (to S.D.K., A.V.Z. and J.Å.), from the Royal Swedish Academy of Sciences (to S.D.K.), and from the Biotechnology and Biological Sciences Research Council/Ministry of Defence, UK (to S.M.). X-ray data were collected at ESRF beamline BM14U, Grenoble, France.

REFERENCES

1 Thanassi, D. G., Saulino, E. T. and Hultgren, S. J. (1998) The chaperone/usher pathway: a major terminal branch of the general secretory pathway. Curr. Opin. Microbiol. **1**, 223–231
2 Knight, S. D., Berglund, J. and Choudhury, D. (2000) Bacterial adhesins: structural studies reveal chaperone function and pilus biogenesis. Curr. Opin. Chem. Biol. **4**, 653–660
3 Sauer, F. G., Knight, S. D., Waksman, G. and Hultgren, S. J. (2000) PapD-like chaperones and pilus biogenesis. Semin. Cell Dev. Biol. **11**, 27–34
4 Sauer, F. G., Barnhart, M., Choudhury, D., Knight, S. D., Waksman, G. and Hultgren, S. J. (2000) Chaperone-assisted pilus assembly and bacterial attachment. Curr. Opin. Struct. Biol. **10**, 548–556
5 Choudhury, D., Thompson, A., Stojanoff, V., Langermann, S., Pinkner, J., Hultgren, S. J. and Knight, S. D. (1999) X-ray structure of the FimC–FimH chaperone–adhesin complex from uropathogenic *Escherichia coli*. Science **285**, 1061–1066
6 Sauer, F. G., Futterer, K., Pinkner, J. S., Dodson, K. W., Hultgren, S. J. and Waksman, G. (1999) Structural basis of chaperone function and pilus biogenesis. Science **285**, 1058–1061
7 Sauer, F. G., Pinkner, J. S., Waksman, G. and Hultgren, S. J. (2002) Chaperone priming of pilus subunits facilitates a topological transition that drives fiber formation. Cell **111**, 543–551
8 Zavialov, A. V., Berglund, J., Pudney, A. F., Fooks, L. J., Ibrahim, T. M., MacIntyre, S. and Knight, S. D. (2003) Structure and biogenesis of the capsular F1 antigen from *Yersinia pestis*: preserved folding energy drives fiber formation. Cell **113**, 587–596
9 Hung, D. L., Knight, S. D., Woods, R. M., Pinkner, J. S. and Hultgren, S. J. (1996) Molecular basis of two subfamilies of immunoglobulin-like chaperones. EMBO J. **15**, 3792–3805
10 Jacob-Dubuisson, F., Striker, R. and Hultgren, S. J. (1994) Chaperone-assisted self-assembly of pili independent of cellular energy. J. Biol. Chem. **269**, 12447–12455
11 Zav'yalov, V. P., Chernovskaya, T. V., Chapman, D. A., Karlyshev, A. V., MacIntyre, S., Zavialov, A. V., Vasiliev, A. M., Denesyuk, A. I., Zav'yalova, G. A., Dudich, I. V. et al. (1997) Influence of the conserved disulphide bond, exposed to the putative binding pocket, on the structure and function of the immunoglobulin-like molecular chaperone Caf1M of *Yersinia pestis*. Biochem. J. **324**, 571–578
12 Hermanns, U., Sebbel, P., Eggli, V. and Glockshuber, R. (2000) Characterization of FimC, a periplasmic assembly factor for biogenesis of type 1 pili in *Escherichia coli*. Biochemistry **39**, 11564–11570
13 Zavialov, A., Berglund, J. and Knight, S. D. (2003) Overexpression, purification, crystallization and preliminary X-ray diffraction analysis of the F1 antigen Caf1M–Caf1 chaperone–subunit pre-assembly complex from *Yersinia pestis*. Acta Crystallogr. Sect. D Biol. Crystallogr. **59**, 359–362
14 Wang, W. and Malcolm, B. A. (2002) Two-stage polymerase chain reaction protocol allowing introduction of multiple mutations, deletions, and insertions, using QuikChange site-directed mutagenesis. Methods Mol. Biol. **182**, 37–43
15 MacIntyre, S., Zyrianova, I. M., Chernovskaya, T. V., Leonard, M., Rudenko, E. G., Zav'yalov, V. P. and Chapman, D. A. (2001) An extended hydrophobic interactive surface of *Yersinia pestis* Caf1M chaperone is essential for subunit binding and F1 capsule assembly. Mol. Microbiol. **39**, 12–25
16 Zavialov, A. V., Kersley, J., Korpela, T., Zav'yalov, V. P., MacIntyre, S. and Knight, S. D. (2002) Donor strand complementation mechanism in the biogenesis of non-pilus systems. Mol. Microbiol. **45**, 983–995
17 Collaborative Computational Project, Number 4 (1994) The CCP4 suite: programs for protein crystallography. Acta Crystallogr. Sect. D Biol. Crystallogr. **50**, 760–763
18 Navaza, J. (1994) AMoRe: an automated package for molecular replacement. Acta Crystallogr. Sect. A Found. Crystallogr. **50**, 157–163
19 Brünger, A. T., Adams, P. D., Clore, G. M., DeLano, W. L., Gros, P., Grosse-Kunstleve, R. W., Jiang, J. S., Kuszewski, J., Nilges, M., Pannu, N. S. et al. (1998) Crystallography & NMR system: a new software suite for macromolecular structure determination. Acta Crystallogr. Sect. D Biol. Crystallogr. **54**, 905–921
20 Privalov, P. L. and Potekhin, S. A. (1986) Scanning microcalorimetry in studying temperature-induced changes in proteins. Methods Enzymol. **131**, 4–51
21 Brandts, J. F. and Lin, L. N. (1990) Study of strong to ultratight protein interactions using differential scanning calorimetry. Biochemistry **29**, 6927–6940
22 Pearlman, D. A., Case, D. A., Caldwell, J. C., Ross, W. R., Cheatham, III, T. E., DeBolt, S., Ferguson, D., Seibel, G. and Kollman, P. (1995) AMBER, a computer program for applying molecular mechanics, normal mode analysis, molecular dynamics and free energy calculations to elucidate the structures and energies of molecules. Comp. Phys. Commun. **91**, 1–41
23 Cornell, W. D., Cieplak, P., Bayly, C. I., Gould, I. R., Merz, Jr, K. M., Ferguson, D. M., Spellmeyer, D. C., Fox, T., Caldwell, J. W. and Kollman, P. A. (1995) A second generation force-field for the simulation of proteins, nucleic-acids, and organic molecules. J. Am. Chem. Soc. **117**, 5179–5197
24 Jorgensen, W. L., Chandrasekhar, J., Madura, J. D., Impey, R. W. and Klein, M. L. (1983) Comparison of simple potential functions for simulating liquid water. J. Chem. Phys. **79**, 926–935
25 Darden, T., York, D. and Pedersen, L. (1993) Particle mesh Ewald: an N.log(N) method for Ewald sums in large systems. J. Chem. Phys. **98**, 10089–10092
26 Vetsch, M., Sebbel, P. and Glockshuber, R. (2002) Chaperone-independent folding of type 1 pilus domains. J. Mol. Biol. **322**, 827–840
27 Jelesarov, I. and Bosshard, H. R. (1999) Isothermal titration calorimetry and differential scanning calorimetry as complementary tools to investigate the energetics of biomolecular recognition. J. Mol. Recognit. **12**, 3–18
28 Sturtevant, J. M. (1987) Biochemical applications of differential scanning calorimetry. Annu. Rev. Phys. Chem. **38**, 463–488
29 Anderson, K. L., Billington, J., Pettigrew, D., Cota, E., Simpson, P., Roversi, P., Chen, H. A., Urvil, P., du Merle, L., Barlow, P. N. et al. (2004) An atomic resolution model for assembly, architecture, and function of the Dr adhesins. Mol. Cell **15**, 647–657
30 Barnhart, M. M., Pinkner, J. S., Soto, G. E., Sauer, F. G., Langermann, S., Waksman, G., Frieden, C. and Hultgren, S. J. (2000) PapD-like chaperones provide the missing information for folding of pilin proteins. Proc. Natl. Acad. Sci. U.S.A. **97**, 7709–7714
31 Abramov, V. M., Vasiliev, A. M., Vasilenko, R. N., Kulikova, N. L., Kosarev, I. V., Khlebnikov, V. S., Ishchenko, A. T., MacIntyre, S., Gillespie, J. R., Khurana, R. et al. (2001) Structural and functional similarity between *Yersinia pestis* capsular protein Caf1 and human interleukin-1β. Biochemistry **40**, 6076–6084
32 Santoro, M. M. and Bolen, D. W. (1988) Unfolding free energy changes determined by the linear extrapolation method. 1. Unfolding of phenylmethanesulfonyl α-chymotrypsin using different denaturants. Biochemistry **27**, 8063–8068
33 Lawrence, M. C. and Colman, P. M. (1993) Shape complementarity at protein/protein interfaces. J. Mol. Biol. **234**, 946–950
34 Makhatadze, G. I. and Privalov, P. L. (1995) Energetics of protein structure. Adv. Protein. Chem. **47**, 307–425
35 Liu, R., Baase, W. A. and Matthews, B. W. (2000) The introduction of strain and its effects on the structure and stability of T4 lysozyme. J. Mol. Biol. **295**, 127–145
36 Jones, C. H., Danese, P. N., Pinkner, J. S., Silhavy, T. J. and Hultgren, S. J. (1997) The chaperone-assisted membrane release and folding pathway is sensed by two signal transduction systems. EMBO J. **16**, 6394–6406
37 Vetsch, M., Puorger, C., Spirig, T., Grauschopf, U., Weber-Ban, E. U. and Glockshuber, R. (2004) Pilus chaperones represent a new type of protein-folding catalyst. Nature (London) **431**, 329–333
38 Soto, G. E., Dodson, K. W., Ogg, D., Liu, C., Heuser, J., Knight, S., Kihlberg, J., Jones, C. H. and Hultgren, S. J. (1998) Periplasmic chaperone recognition motif of subunits mediates quaternary interactions in the pilus. EMBO J. **17**, 6155–6167

Received 11 March 2005; accepted 31 March 2005
Published as BJ Immediate Publication 31 March 2005, DOI 10.1042/BJ20050426